


# Renal epithelioid angiomyolipoma: magnetic resonance imaging characteristics

Xinying Cong,<sup>1,2</sup> Jin Zhang,<sup>1</sup> Xiaojuan Xu,<sup>1</sup> Miaomiao Zhang,<sup>1</sup> Yan Chen<sup>1</sup> 

<sup>1</sup>National Cancer Center/Cancer Hospital, Chinese Academy of Medical Sciences and Peking Union Medical College, Beijing 100021, China

<sup>2</sup>Present address: China Rehabilitation Research Center, Beijing 100068, China

## Abstract

**Objective:** The aim of the study was to analyze MR imaging features of renal epithelioid angiomyolipoma (EAML).

**Methods:** This study included 17 patients with histopathologically confirmed renal EAML who underwent renal MRI scanning before radical or partial nephrectomy. MR images were retrospectively reviewed and correlated with pathological findings.

**Result:** Fifteen lesions (88.2%) appeared as round or oval. The tumor-kidney interface was round in 14 lesions (82.4%). Fifteen tumors (88.2%) presented mainly isointensity on T1WI, and eleven tumors (64.7%) presented mainly hypointensity on T2WI. Twelve lesions (70.6%) showed restricted diffusion on DWI, and the mean ADC value was  $1.23 \pm 0.28 \times 10^{-3} \text{mm}^2/\text{s}$ . Minimal fat component was identified as loss of signal intensity on opposed-phase MR images in 6 cases (35.3%). Sixteen lesions (100%) demonstrated inhomogeneous enhancement, and 7 of 16 masses (43.8%) showed reticular enhancement. Rapid wash-in and wash-out enhancement was seen in 13 masses (81.3%). In the corticomedullary phase, the mass showed markedly enhancement in 14 cases (87.5%). The irregular vessels and hemorrhage were detected in 4 cases (23.5%) and 7 cases (41.2%), respectively. One patient (5.9%) had a lymph node involvement at initial diagnosis, and showed distant metastasis after operation. In the immunohistochemical analysis, 15 tumors (88.2%) were positive for melanocytic marker (HMB45 or Melan-A), and all cases (100%) were negative for epithelial-associated markers (CK or AE1/AE3).

**Conclusion:** The presence of hypointensity on T2WI, restricted diffusion on DWI, round tumor-kidney interface, reticular, and marked enhancement (rapid wash-in

and wash-out) should further raise suspicion for renal EAML. The diagnosis may be confirmed by pathological analysis.

**Key words:** Perivascular epithelioid cell neoplasms—Angiomyolipoma—Magnetic resonance imaging—Renal neoplasms—Epithelioid angiomyolipoma

Angiomyolipoma (AML) is the most common benign mesenchymal renal neoplasm composed of variable proportions of abnormal thick-walled blood vessels, spindle cells, epithelioid smooth muscle cells, and adipose tissue [1]. Epithelioid angiomyolipoma (EAML) was first described as a rare variant of AML by Martignoni et al. and Mai et al. in 1995 and 1996, respectively [2, 3]. Renal EAML is considered as a new category of kidney neoplasms by the World Health Organization Classification of Renal Neoplasms in 2016, and was classified as a potentially malignant mesenchymal neoplasm with possible lymph node metastasis, local recurrence, and distant metastasis [4]. It belongs to a family of perivascular epithelioid cell tumors (PEComas). The histologic features of EAML are different from those of classical AML, it instead consists predominately of epithelioid cells. The new classification of tumors of the kidney determined the diagnostic criteria as having epithelioid portion of more than 80% of the tumor [4]. The coexistence of EAML with tuberous sclerosis complex (TSC) has been provided by some case reports and several large series [5].

Classical AML can be easily diagnosed when the lesion is radiologically classic, with an identifiable adipose tissue component [6, 7]. However, EAML contain minimal or no fat to be characterized using conventional CT/MRI, which may result in misdiagnosis [8–11]. The radiological appearance of renal EAML has not been

well described or discussed in the literature so far [8–11]. In the present study, we aimed to retrospectively review MRI imaging characteristics of 17 cases of renal EAML in a single institution and provided a review of the literature. To our knowledge, this is the largest case series about correlation of MR imaging features and pathologic findings following the 2016 WHO new pathologic criteria of renal EAML.

## Methods

### *Patients*

This single institution retrospective study was approved by the institutional review board, and informed consent for Magnetic Resonance Imaging scanning had routinely been obtained from each individual included in this study. Between January 2005 and May 2017, seventeen patients (13 women, 4 men) aged 23–61 years (mean 38.4 years) were surgically and pathologically diagnosed as renal EAML. Eight patients underwent radical nephrectomy, and nine patients underwent partial nephrectomy. MRI examination was performed in all cases before surgery. All the patients' records including disease associations, clinical presentation, follow-up information, MR imaging features, and pathological findings were reviewed and summarized.

### *MRI protocol*

MR examinations were performed with the patient in a supine position by using a 3.0-T imaging unit (GE Signa Excite HDx GEHC/GEHC) with a body phased-array coil. For the MR images, the following sequences were obtained: axial and coronal T2-weighted fast spin echo sequences, transverse T1-weighted dual-echo in-phase and out-of-phase sequences, transverse diffusion weighted images (DWI,  $b = 0, 800 \text{ s/mm}^2$ ), and three-dimensional fat-saturated T1-weighted dynamic contrast-enhanced sequences. Gadopentetate dimeglumine (0.2 mmol per kilogram body weight) was injected intravenously at a flow rate of 3 ml/s by using a power injector and followed by a 20-ml saline flush. The mask images were obtained before contrast agent injection. The post-contrast acquisition of corticomedullary phase was obtained at 25–30 s, the nephrographic phase at 60–70 s, and the urographic phase at 180 s. Sixteen cases underwent both MRI plain scanning and multi-phases dynamic enhancement scanning, one case underwent MRI plain scanning only.

### *MRI analysis*

T1-weighted MR images, T2-weighted MR images, diffusion weighted images with subsequent apparent diffusion coefficient (ADC) maps measurement, and dynamic contrast-enhanced MR images were evaluated in con-

sensus retrospectively by two genitourinary radiologists with 10 and 3 years of experience in kidney MR imaging respectively.

### *Qualitative analysis*

Tumor location, tumor size, growth pattern, signal intensity, existence of fat, heterogeneity, the pattern, and degree of enhancement were evaluated in all cases. For both T1-weighted and T2-weighted images, the signal intensity of normal renal cortex was used as reference for evaluating the signal intensity of the tumor: “hypointensity” when lower than that of normal renal cortex, “isointensity” when similar, “hyperintensity” when higher. Restricted diffusion was defined as showing high signal intensity on diffusion weighted images with high  $b$  values and corresponding lower apparent diffusion coefficient (ADC) values [12, 13]. Compared with the surrounding normal renal cortex in the corticomedullary phase, the degree of enhancement was classified into three levels. If the enhancement of tumor was similar to that of the normal renal cortex, the tumor was classified as marked enhancement; if no or very little enhancement was observed, the tumor was classified as mild enhancement; if enhancement was intermediate between marked enhancement and mild enhancement, the tumor was classified as moderate enhancement.

### *Quantitative DWI*

The region of interest (ROI) analysis of apparent diffusion coefficient maps from DWI data was performed for each renal mass by using Advantage workstation (version 4.4; GE Medical Systems). The ROI was drawn in the solid portion of lesion, avoiding regions of cystic degeneration, necrosis, and haemorrhage. An average of three measurements per lesion were performed. The ADC value was recorded as mean and standard deviation.

### *Pathologic evaluation*

Initial histopathological diagnosis was available for all patients after radical or partial nephrectomy. Gross pathological characteristics were assessed. Histological observation and immunohistochemical staining of melanocytic markers and epithelial-associated markers were performed to confirm the pathological diagnosis.

## Results

### *Clinical information*

The clinical features of all cases and follow-up data are shown in Table 1. In our study, ten patients (58.8%) showed an insidious onset, and tumors were incidentally discovered in routine physical examinations. Five patients (29.4%) complained of abdominal pain and dis-

**Table 1.** Demographics, presentation, and follow-up data of 17 patients with renal EAML

Patient age (year), mean (range)	38.4 (23–61)
Sex distribution	
Female	76.5% (13/17)
Male	23.5% (4/17)
Presentation	
Asymptomatic	58.8% (10/17)
Abdominal pain and discomfort	29.4% (5/17)
Weight loss	5.9% (1/17)
Hematuria	5.9% (1/17)
With TSC	0/17
Metastasis at the time of diagnosis	5.9% (1/17)
Metastasis during follow-up	5.9% (1/17)
Follow-up period (m), mean (range)	46.9 (7–116)

comfort. One patient (5.9%) had weight loss, and one patient (5.9%) presented as painless, gross hematuria. None of all cases had history of tuberous sclerosis complex. Follow-up of all cases lasted 7–116 months (mean, 46.9 months). The patient with para-caval lymph nodes involvement at the time of initial diagnosis showed distant metastasis 4 months post operation. CT imaging displayed the metastasis to retroperitoneal nodes, liver, and right iliac fossa (Fig. 4E–G). All other patients did not show any evidence of recurrence or metastasis.

### MRI findings

The MR imaging characteristics are summarized in Table 2. The lesions were in right kidney in 9 cases (52.9%) and left in 8 cases (47.1%). The tumor diameter varied from 0.9 to 16.2 cm (mean, 6.9 cm). Fifteen lesions (88.2%) appeared as round or oval, two lesions (11.8%) as lobulated. The tumor-kidney interface was round in fourteen lesions (82.4%) (Fig. 1F). Angular interface was observed in the other 3 lesions (17.6%). Thirteen cases (76.5%) showed exophytic masses, and four lesions (23.5%) were within kidney contours. Compared with the surrounding normal renal cortex, 15 tumors (88.2%) presented mainly isointensity on T1-weighted image, and 11 tumors (64.7%) presented mainly hypointensity on T2-weighted image or fat saturated T2-weighted image (Fig. 1A–C). Twelve lesions (70.6%) showed hyperintensity on DWI, and the corresponding apparent diffusion coefficient (ADC) values decreased (Fig. 1D–E). The mean ADC value of all lesions was  $1.23 \pm 0.28 \times 10^{-3} \text{ mm}^2/\text{s}$ .

The component of fat was identified as loss of signal intensity on opposed-phase gradient-echo MR images in 6 cases (35.3%) (Fig. 4B). The tortuous and irregular vessels in the lesion were detected in 4 cases (23.5%) (Fig. 2), and lesions with hemorrhage were hyperintensity on T1-weighted images in 7 cases (41.2%) (Fig. 4A). Variable necrosis or cystic areas were present in 10 cases (58.8%). One patient (5.9%) had a para-caval lymph

**Table 2.** Radiologic characteristics in 17 cases of renal EAML

Location	
Right kidney	52.9% (9/17)
Left kidney	47.1% (8/17)
Size (cm), mean (range)	6.9 (0.9–16.2)
Shape	
Round/oval	88.2% (15/17)
Lobulated	11.8% (2/17)
Tumor-kidney interface	
Round	82.4% (14/17)
Angular	17.6% (3/17)
Growth pattern	
Exophytic	76.5% (13/17)
Within kidney contours	23.5% (4/17)
T1WI	
Mainly isointensity	88.2% (15/17)
Other	11.8% (2/17)
T2WI	
Mainly hypointensity	64.7% (11/17)
Other	35.3% (6/17)
DWI	
Hyperintensity	70.6% (12/17)
Other	29.4% (5/17)
Heterogeneous enhancement	100% (16/16)
Reticular	43.8% (7/16)
Other	56.2% (9/16)
Pattern of enhancement	
Wash-in and wash-out	81.3% (13/16)
Persistent enhancement	6.2% (1/16)
Delayed enhancement	12.5% (2/16)
Degree of enhancement in the cortico medullary phase	
Marked enhancement	87.5% (14/16)
Moderate enhancement	12.5% (2/16)
Fat component	
Identified on opposed-phase gradient-echo	35.3% (6/17)
Necrosis or cystic change	58.8% (10/17)
Tortuous and irregular vessels within tumor	23.5% (4/17)
Hemorrhage	41.2% (7/17)
Renal capsule or perinephric fat extension	52.9% (9/17)
Lymph nodes involvement	5.9% (1/17)
Tumor thrombus in renal vein	11.8% (2/17)

nodes involvement at the time of diagnosis (Fig. 4). Tumor thrombus extending into the right renal vein was seen in 2 cases (11.8%) (Fig. 3).

Sixteen lesions (100%) demonstrated inhomogeneous enhancement, and 7 of 16 (43.8%) masses showed reticular enhancement (Figs. 1F, G and 4C, D). Thirteen masses (81.3%) enhanced similar to the normal renal cortex in the corticomedullary phase, and obviously decreased enhancement in the nephrographic phase, which can be defined as wash-in and wash-out (Fig. 1F, G). One case (6.2%) demonstrated persistent enhancement. In two cases (12.5%), the lesions displayed prolonged enhancement. In the corticomedullary phase, the mass showed markedly enhancement in 14 cases (87.5%), and moderately enhancement in the other 2 tumors (12.5%).

### Pathologic findings

Histopathological diagnosis of renal EAML was made in all the 17 cases. The percentage of epithelioid component ranged from 80% to 100%. Grossly all cases were typically solid, and complete capsule was observed in six

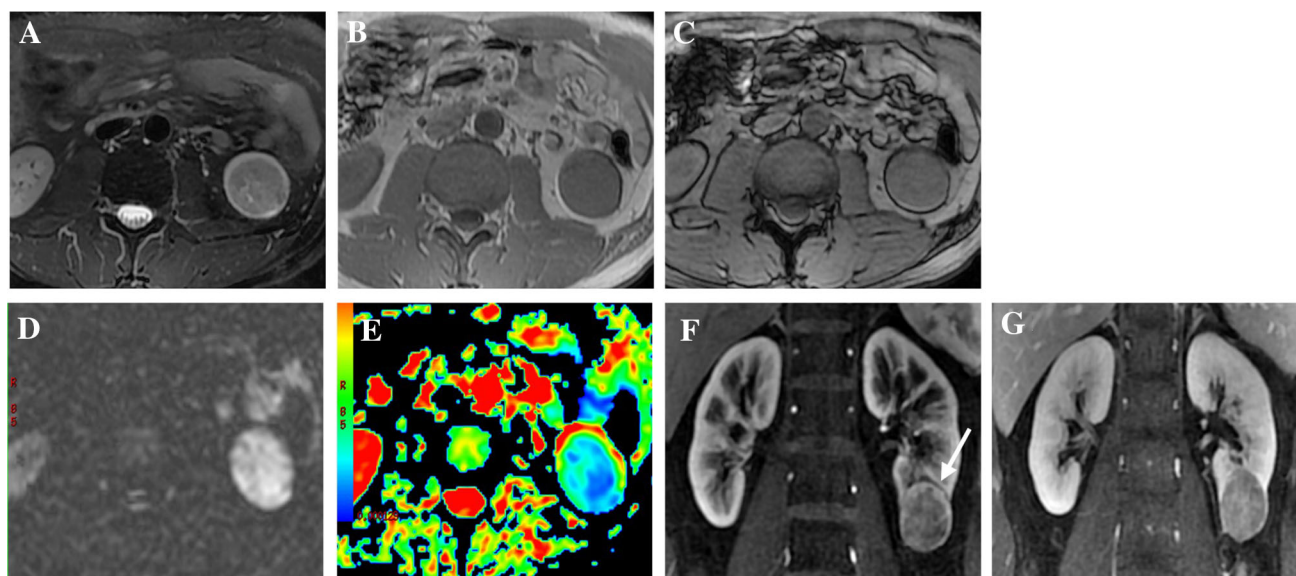


**Fig. 1.** A 25-year-old woman with renal EAML. It shows isointensity on axial in/opposed phase T1-weighted images (**B, C**), mainly hypointensity on axial fat saturated T2-weighted imaging (**A**). Axial DW imaging (**D**) shows a renal tumor with remarkable high signal intensity. Axial ADC map

(**E**) shows obviously diffusion restriction of the renal tumor. Contrast-enhanced coronal T1-weighted imaging (**F, G**) shows the mass with reticular, marked enhancement (rapid wash-in and wash-out), and the mass has a round interface with kidney (arrow).

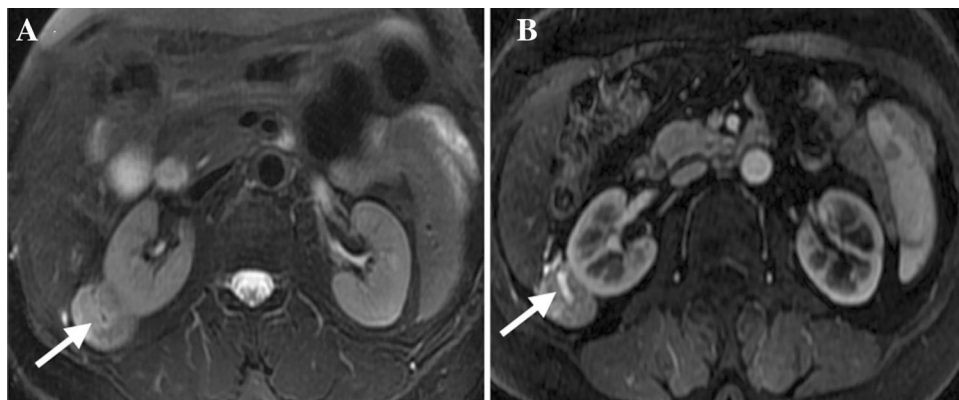


**Fig. 2.** A 56-year-old woman with renal EAML. Axial fat-saturated T2-weighted imaging (**A**) shows vascular flow voids in mass (arrow). Contrast-enhanced axial T1-weighted imaging (**B**) demonstrates the tumor with enhancing vessel (arrow).

cases (35.3%). Variable necrosis or cystic areas were present in 12 cases (70.6%). Haemorrhage was seen in 9 cases (52.9%). Invasion of the renal capsule and perirenal fat was present in 7 cases (41.2%) and 2 cases (11.8%), respectively. Lymph node metastasis was seen in one patient (5.9%). Renal vein involvement was present in 2 cases (11.8%). For the immunohistochemical analysis, 15 tumors (88.2%) were positive for melanocytic marker (HMB45 or Melan-A). All cases (100%) were negative for epithelial-associated markers (CK or AE1/AE3). The positivity for Ki-67 ranged from 1% to 10% in 11 cases.

## Discussion

As a new category of renal tumors, EAML has been regarded as a potentially malignant mesenchymal neo-

plasm by the World Health Organization Classification of Renal Neoplasms in 2016 [4]. The clinical presentations of EAML were varied and non-specific. In our series, most of renal EAMLs were incidentally detected by imaging. Its main clinical symptoms included chronic intermittent abdominal discomfort, hematuria, loss of weight, and so on. Like classical AML, EAML has been described in patients with and without evidence of TSC, as well as in the TSC2/PKD1 contiguous gene syndrome [4, 5]. In a series of 194 cases, Aydin et al. described that patients with EAML were more commonly associated with TSC, compared to those without epithelioid component (26.7% vs. 6.7%) [5]. In a series of 10 patients, Cui et al. found no patient with TSC [8]. In our series, none of all the cases had a history of TSC. Meanwhile, renal



**Fig. 3.** A 23-year-old man with renal EAML. Coronal contrast-enhanced T1-weighted imaging shows a renal mass with tumor thrombus extending into the right renal vein.

EAML is more likely to occur in females in our study, which is concordant with previously published literature [9, 10, 14, 15].

Verma et al. tried to categorize the exophytic renal mass on the basis of an angular or round interface with the renal parenchyma [16]. In our study, the tumor-kidney interface was round in 14 lesions (82.4%). We have noted that most of EAML have a round interface with kidney, whereas classical AML and fat-poor AML have an angular interface, with a definable apex within renal parenchyma [16, 17]. In a series of 20 patients with fat-poor AML, nine tumors showed angular interface with renal parenchyma [18]. The results of our study suggest that the presence of a round interface with the renal parenchyma supports the diagnosis of EAML.

Tsukada et al. had showed that hypointensity on T2-weighted image or fat saturated T2-weighted image is a characteristic finding of renal EAML [9]. Eleven cases (64.7%) presented mainly hypointensity on T2-weighted image or fat saturated T2-weighted image. To our knowledge, hypointensity on T2-weighted image could also be observed in papillary RCC, chromophobe RCC and minimal fat AML [19–23]. However, most of these renal tumors have some unique imaging features that may allow differentiation from EAML.

As we all known, classical AML can be easily diagnosed by detecting fat components on radiologic imaging. However, due to the lack of visible fat on imaging,

renal EAMLs are often misdiagnosed as other renal neoplasms, such as renal cell carcinoma, sarcomas, fat-poor AML [5]. Cui and Jitsuro Tsukada identified no intratumoral fat in all cases of their series [8, 9]. In a series of nine patients, Froemming et al. found minor components of fat in six patients [10]. In our study, the minimal fat component was identified as loss of signal intensity on opposed-phase gradient-echo MR images in six cases (35.3%). This finding suggests that most renal EAML has insufficient fat to be characterized, and signal intensity drop on opposed-phase gradient-echo MR images is helpful to detect microscopic fat, which is a suggestive imaging finding.

The tortuous and irregular vessels were present in 4 lesions (23.5%). Like classical AML, the vessel is poorly organized, sometimes which could cause hemorrhage [1]. Several studies of classical AML have reported that thresholds of 4 cm for tumor size and 5 mm for size of aneurysm have association with future bleeding [24]. In our series, hemorrhage was observed in seven cases (41.2%). In a series of nine patients, Froemming et al. reported four cases of renal EAMLs with acute hemorrhage, and regarded it as a suggestive imaging finding [10]. But it is not a specific finding of EAML, hemorrhage on T1-weighted image could also be observed in classical AML, RCC, and other causes of hemorrhage [25–27].

To date, only a few articles have reported the enhancement characteristic of EAML. In our series, sixteen lesions (100%) demonstrated inhomogeneous enhancement, and 7 of 16 masses (43.8%) showed reticular enhancement which were different from clear cell RCC. Thirteen masses (81.3%) enhanced similar to the normal renal cortex in the corticomedullary phase, and obviously decreased enhancement in the nephrographic phase. The enhancement degree was marked enhancement in fourteen cases (87.5%) in corticomedullary phase. To sum up, the pattern and degree of enhancement of renal EAML may mimic the MRI findings of clear cell RCC, but the reticular enhancement is a suggestive characteristic of renal EAML.

In our series, twelve lesions (70.6%) showed restricted diffusion on diffusion weighted images. The mean ADC value of all renal EAML lesions in our study was  $1.23 \pm 0.28 \times 10^{-3} \text{mm}^2/\text{s}$ . This finding may be explained by tissue cellularity and degree of cell membrane integrity. In common renal lesions, published ADC values varied from  $1.42 \times 10^{-3}$  to  $1.84 \times 10^{-3} \text{mm}^2/\text{s}$  in clear cell RCCs,  $0.74 \times 10^{-3}$  to  $1.46 \times 10^{-3} \text{mm}^2/\text{s}$  in classical AMLs, and  $0.67 \times 10^{-3}$  to  $1.26 \times 10^{-3} \text{mm}^2/\text{s}$  in fat poor AMLs, respectively [28–32]. Our study derived lower ADC value for EAML than for clear cell RCC, while there was overlap in ADC values between EAML and AML (including classical AML and fat-poor AML). Further work is needed to explore whether there

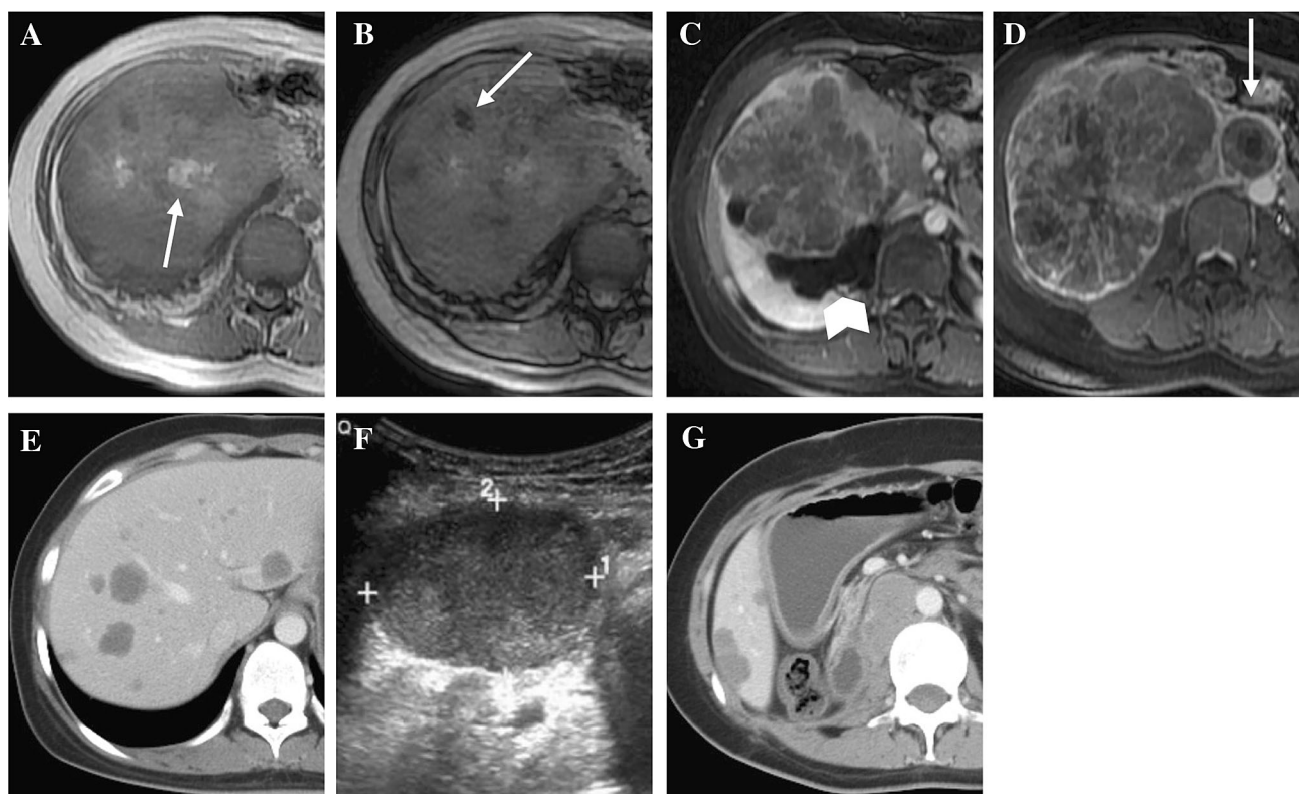


**Fig. 4.** A 25-year-old woman with renal EAML and lymph nodes involvement. Axial in/opposed phase T1-weighted images (**A**, **B**) show loss of signal intensity and patchy hyperintensity, which indicates fat component and hemorrhage respectively (arrows). Axial contrast-enhanced T1-weighted images (**C**, **D**) show a large renal tumor and en-

larged retroperitoneal lymph node (arrow) with reticular heterogeneous enhancement, and secondary pelvicaliceal dilation is observed (arrowhead). Distant metastasis to liver, right iliac fossa, and para-caval lymph node are detected 4 months after complete resection of all lesions (**E–G**).

is statistically significant differences in ADC values between EAML and other renal tumors.

In our study, one patient who had para-caval lymph node involvement at initial diagnosis showed distant metastasis after complete surgical resection, and died of this disease finally. Before operation, MR images showed a huge heterogeneous tumor originated from right kidney with hemorrhage and necrosis. An enlarged retroperitoneal lymph node was also observed. The tumor and enlarged lymph node enhanced similar to the normal renal cortex in the corticomedullary phase, and obviously decreased enhancement in the nephrographic phase. This disease progression may be associated with large tumor size, presence of necrosis, lymph node metastasis and involvement of perinephric fat tissue, which is concordant with adverse prognostic parameters for EAML proposed by Nese et al. [33]. In recent years, there have been some different case reports and series of renal EAML with metastatic and aggressive behavior [14, 15, 33, 34]. The most common metastatic sites of EAML are liver, followed by lung and other unusual sites [14, 15, 33, 34]. The rate of recurrence or metastasis

is not consistent among different studies, with a wide range from 0% to 51% [5, 14, 33, 34].

Because of potentially malignant behavior of EAML, it should be managed as other malignant renal tumors are [35]. Accordingly, surgical resection is justified for patients. Meanwhile patients with renal EAML require a careful follow-up for a long period. Treatment of renal EAML patients with mTOR pathway inhibitor, such as sirolimus or temsirolimus, had shown tumor regression and favorable outcome in recent studies [36–38]. Consequently, radiologic interpretation of the renal EAML can be helpful in planning treatment and evaluating treatment response.

To date, a variety of imaging features have been described for the characterization of fat-poor AML. Our study showed that most of MRI findings are significant overlap between fat-poor AML and EAML. We suggest that renal EAML should be considered when a patient presents larger renal mass with round tumor-kidney interface, especially with lymph node involvement. Our results also indicate that in and opposed-phase gradient-echo MR images is necessary, which is helpful to detect

microscopic fat and differentiate EAML and poor-fat AML from other renal tumors.

The present study had several limitations. Firstly, it was a retrospective single-center study. Secondly, it has mainly focused on the radiological appearance of renal EAML, while comparative study between imaging features of renal EAML and other renal tumors did not be included. Thirdly, because only one patient showed disease progression, it is not enough to compare the MR findings to the benign or malignant behavior of EAML.

## Conclusion

Most of patients with renal EAML are women and have no characteristic clinical manifestations. The radiological appearance of EAML has a tendency to be mainly hypointensity on T2WI, restricted diffusion on DWI. Inhomogeneous marked enhancement in the corticomedullary phase, especially reticular enhancement and rapid wash-in and wash-out are also suggestive imaging findings. The presence of a round interface with the normal renal parenchyma supports the diagnosis of EAML. Renal EAML has minor or no components of identifiable fat on imaging. In general, most of renal EAMLs have benign biological behavior, but it may have malignant potential with recurrence and metastasis.

### Compliance with ethical standards

**Funding** No funding was received for this study.

**Conflict of interest** The authors declare that they have no conflict of interest.

**Ethical approval** Informed consent was not required as it was a retrospective data analysis of MRI exams that had been acquired as part of clinical routine. Informed consent for Magnetic Resonance Imaging exams had routinely been obtained from each individual included in this study. This study is in accordance with the ethical standards of the institutional and national research committee and with the 1964 Helsinki declaration and its later amendments or comparable ethical standards.

## References

- Martignoni G, Reuter VE, Fletcher CDM, World Health Organization (2016) *Angiomyolipoma of World Health Organization Classification of Tumours of the Urinary System and Male Genital Organs*. Lyon: IARC Press, pp 62–65
- Martignoni G, Bonetti F (1995) Renal epithelioid oxyphilic neoplasm (REON), a pleomorphic variant of renal angiomyolipoma. *Int J Surg Pathol* 2:539
- Mai KT, Collins JP (1996) Epithelioid cell variant of renal angiomyolipoma. *Histopathology* 28:277–280
- Martignoni G, Reuter VE, Fletcher CDM, World Health Organization (2016) *Epithelioid angiomyolipoma of World Health Organization Classification of Tumours of the Urinary System and Male Genital Organs*. World Health Organization. Lyon: IARC Press, pp 65–66
- Aydin H, Magi-Galluzzi C, Lane BR, et al. (2009) Renal angiomyolipoma clinicopathologic study of 194 cases with emphasis on the epithelioid histology and tuberous sclerosis association. *Am J Surg Pathol* 33(2):289–297
- Jinzaki M, Silverman SG, Akita H, et al. (2014) Renal angiomyolipoma: a radiological classification and update on recent developments in diagnosis and management. *Abdom Imaging* 39(3):588–604
- Israel GM, Hindman N, Hecht E, Krinsky G (2005) The use of opposed-phase chemical shift MRI in the diagnosis of renal angiomyolipomas. *AJR Am J Roentgenol* 184(6):1868–1872
- Cui L, Zhang JG, Hu XY, et al. (2012) CT imaging and histopathological features of renal epithelioid angiomyolipomas. *Clin Radiol* 67(12):e77–e82
- Tsakada J, Jinzaki M, Yao M, et al. (2013) Epithelioid angiomyolipoma of the kidney: radiological imaging. *Int J Urol* 20(11):1105–1111
- Froemming AT, Boland J, Cheville J, Takahashi N, Kawashima A (2013) Renal epithelioid angiomyolipoma: imaging characteristics in nine cases with radiologic-pathologic correlation and review of the literature. *AJR Am. J. Roentgenol* 200(2):W178–W186
- Zhong Y, Shen Y, Pan J, et al. (2017) Renal epithelioid angiomyolipoma: MRI findings. *Radiol Med* 122(11):814–821
- Thoeny HC, De Keyzer F (2007) Extracranial applications of diffusion-weighted magnetic resonance imaging. *Eur Radiol* 17(6):1385–1393
- Sufana Iancu A, Colin P, Puech P, et al. (2013) Significance of ADC value for detection and characterization of urothelial carcinoma of upper urinary tract using diffusion-weighted MRI. *World J Urol* 31(1):13–19
- Brimo F, Robinson B, Guo C, et al. (2010) Renal epithelioid angiomyolipoma with atypia: a series of 40 cases with emphasis on clinicopathologic prognostic indicators of malignancy. *Am J Surg Pathol* 34(5):715–722
- Faraji H, Nguyen BN, Mai KT (2009) Renal epithelioid angiomyolipoma: a study of six cases and a meta-analytic study. Development of criteria for screening the entity with prognostic significance. *Histopathology* 55(5):525–534
- Verma SK, Mitchell DG, Yang R, et al. (2010) Exophytic renal masses: angular interface with renal parenchyma for distinguishing benign from malignant lesions at MR imaging. *Radiology* 255(2):501–507
- Jinzaki M, Silverman SG, Akita H, Mikami S, Oya M (2017) Diagnosis of renal angiomyolipomas: classic, fat-poor, and epithelioid types. *Semin Ultrasound CT MR* 38(1):37–46
- Chen Y, Zhu Z, Dai JR, et al. (2010) Imaging findings of benign renal angiomyolipoma with minimal fat content. *Chin Clin Med Imaging* 21(10):705–708
- Vikram R, Ng CS, Tamboli P, et al. (2009) Papillary renal cell carcinoma radiologic-pathologic correlation and spectrum of disease. *Radiographics* 29(3):741–754
- Pedrosa I, Sun MR, Spencer M, et al. (2008) MR imaging of renal masses: correlation with findings at surgery and pathologic analysis. *Radiographics* 28(4):985–1003
- Chung MS, Choi HJ, Kim MH, Cho KS (2014) Comparison of t2-weighted MRI with and without fat suppression for differentiating renal angiomyolipomas without visible fat from other renal tumors. *AJR Am J Roentgenol* 202:765–771
- Low G, Sahi K, Dhliwayo H (2012) Low T2 signal intensity on magnetic resonance imaging: a feature of minimal fat angiomyolipomas. *Int J Urol* 19(1):90–91
- Kim Y, Sung DJ, Sim KC, et al. (2017) Renal tumors with low signal intensities on T2-weighted MR image: radiologic-pathologic correlation. *Abdom Radiol* 42(8):2108–2118
- Yamakado K, Tanaka N, Nakagawa T, et al. (2002) Renal angiomyolipoma: relationships between tumor size, aneurysm formation, and rupture. *Radiology* 225(1):78–82
- Schieda N, Kielar AZ, Al McInnes MD, Flood TA (2015) Ten uncommon and unusual variants of renal angiomyolipoma (AML): radiologic-pathologic correlation. *Clin Radiol* 70(2):206–220
- Beddy P, Genega EM, Ngo L, et al. (2014) Tumor necrosis on magnetic resonance imaging correlates with aggressive histology and disease progression in clear cell renal cell carcinoma. *Clin Genitourin Cancer* 12:55–62
- Corr P, Yang WT, Tan I (1994) Spontaneous haemorrhage from renal angiomyolipomata. *Australas Radiol* 38:132–134
- Wang H, Cheng L, Zhang X, et al. (2010) Renal cell carcinoma: diffusion-weighted MR imaging for subtype differentiation at 3.0 T. *Radiology* 257(1):135–143

29. Sasamori H, Saiki M, Suyama J, et al. (2014) Utility of apparent diffusion coefficients in the evaluation of solid renal tumors at 3T. *Magn Reson Med Sci* 13(2):89–95
30. Cornelis F, Tricaud E, Lasserre AS, et al. (2014) Routinely performed multiparametric magnetic resonance imaging helps to differentiate common subtypes of renal tumours. *Eur Radiol*. 24(5):1068–1080
31. Taouli B, Thakur RK, Mannelli L, et al. (2009) Renal lesions: characterization with diffusion-weighted imaging versus contrast-enhanced MR imaging. *Radiology*. 251(2):398–407
32. Squillaci E, Manenti G, Di Stefano F, et al. (2004) Diffusion-weighted MR imaging in the evaluation of renal tumours. *J Exp Clin Cancer Res* 23(39–45):24
33. Nese N, Martignoni G, Fletcher CD, et al. (2011) Pure epithelioid PE comas (SO-called epithelioid angiomyolipoma) of the KIDNEY: a clinicopathologic study of 41 cases: detailed assessment of morphology and risk stratification. *Am J Surg Pathol* 35(2):161–176
34. Lei JH, Liu LR, Wei Q, et al. (2015) A four-year follow-up study of renal epithelioid angiomyolipoma: a multi-center experience and literature review. *Sci Rep* 5:10030
35. Serrano Frago P, Camisón CDAA, Sanz MJG, et al. (2006) Controversies related to epithelioid variant of renal angiomyolipoma: a review of the literature. *Urology* 67(846):e843–e845
36. Shitara K, Yatabe Y, Mizota A, et al. (2011) Dramatic tumor response to everolimus for malignant epithelioid angiomyolipoma. *Jpn J Clin Oncol* 41(6):814–816
37. Wolff N, Kabbani W, Bradley T, et al. (2010) Sirolimus and temsirolimus for epithelioid angiomyolipoma. *J Clin Oncol* 28:e65–e68
38. Shitara K, Yatabe Y, Mizota A, et al. (2011) Dramatic tumor response to everolimus for malignant epithelioid angiomyolipoma. *Jpn J Clin Oncol* 41:814–816